Creation and application of future typical weather files in the evaluation of indoor overheating in free-floating buildings

Obaidullah Yaqubi, Auline Rodler, Sihem Guernouti, Marjorie Musy

Creation and application of future typical weather files in the evaluation of indoor overheating in free-floating buildings

Obaidullah YAQUBI[1;2;3], Auline RODLER[1;2,4], Sihem GUERNOUTI[1;2;4], Marjorie MUSY[1;2;4],

[1]Equipe de recherche BPE, Cerema, Nantes, France

[2]Institut de Recherche en Sciences et Techniques de la Ville (IRSTV), Nantes, France

[3]Nantes Université, Ecole Centrale Nantes, CNRS, GeM, UMR 6183, F-44000 Nantes, France

[4]CNRS UMR 5271, LOCIE, Université Savoie Mont Blanc, Chambéry, France

Corresponding author:

O. YAQUBI

9 rue René Viviani - BP 46223, 44262 Nantes, Cedex 2, France

obaidullahya@gmail.com

obaidullah.yaqubi@cerema.fr

Abstract

Expected Global warming and heatwaves coupled with the urban heat island effect (UHI) can overheat indoor environments of free-floating buildings in temperate climate regions. Overheating assessment requires practitioners to use appropriate climate data and suitable measurement indices. The aim of this article is first, to propose a practical approach to generate yearly and typical ready-to-use future typical weather datasets (FTWY) using high-resolution Regional Climate Model (RCM) data from Coordinated Regional Climate Downscaling Experiment (CORDEX), and second, investigate the potential of FTWYs in the assessment of indoor overheating, considering UHI effect.

To achieve these objectives, three dynamically downscaled (DDS) FTWYs generated from RCMs (IPSL-SMHI, CNRM-ALADIN, MPI-REMO) were compared with one statistically downscaled (ESD) FTWY from Meteonorm, and observed heatwave weather data of 2003. Comparative analysis was performed in two stages: comparison of monthly statistical distribution of climate variables, and analysis of heatwave presence. Urban weather generator (UWG) was used to project UHI effect on two weather files for two buildings, and three overheating measurement indices were used to exploit results. Comparative analysis of weather files show that temperature in a FTWY in the medium future (2040 -2070) is likely not as intense as the heatwave of 2003 for Nantes. Results also confirm that it is better to use two weather files, and at least two overheating indices to obtain reliable outputs. This study also revealed that indoor overheating is not limited to densely built areas where impact of UHI is highest; buildings located in sparsely built neighbourhoods are also at risk.

1 Introduction

1.1 Climate change & extreme weather events

2011-2020 was the warmest decade on record and the global average temperature in 2020 was approximately 14.9 ° C, which is 1.2°C higher than the pre-industrial (1850-1900) level (WMO 2020). The projections of IPCC in their latest reports warns that even with the best estimates, regardless of what emission scenario is considered, the warming will reach 1.5°C before 2040 (IPCC 2021). National Climate Assessment report states that the number and strength of heatwaves, heavy downpours, and major hurricanes have increased over the last decades and will continue to do so in the future. This increase will disrupt and damage critical infrastructures and vitality of communities, putting vulnerable population disproportionately at risk of climate-related adverse consequences (Doherty et al. 2018).

Europe in particular is more likely to be affected by heatwaves and cold snaps compared to other extreme weather events such as hurricanes that form in tropical and subtropical latitudes.

An example is the exceptional heatwave in the summer of 2003 that resulted in at least 30,000 excess deaths in Europe, of which nearly 15,000 were in France, between August 1 and 20, 2003 (Wagner 2018).

Heatwaves simulated using EURO-CORDEX regional multi-model demonstrate that under future climate conditions, the frequency, duration and intensity of heatwaves will increase across France and other parts of Europe. Heatwave events could occur during a larger span of summertime and the 2003 event would be a typical event by the end of the century (Ouzeau et al. 2016).

1.2 Extreme weather events and cities

Influences of changing frequencies and intensities of extreme weather events are amplified in the urban areas by a distinct urban microclimate feature known as *urban heat*

island (UHI) effect. This effect is characterized by higher temperatures within the build-up urban area as compared to rural surroundings (Pyrgou et al. 2017). UHI is the result of many factors that modify the climatic exchanges in the city: shape and density of urban fabric, thermo-physical specifications of artificial urban surfaces and heat generated from anthropogenic human activities. These factors change the urban energy balance by entrapping solar radiation, changing humidity and intensity of air circulation, increasing thermal storage capacity, and decreasing the latent heat transfer due to the reduced presence of vegetation and water bodies. As a result, urban air and surface temperatures cool down slowly in the evening, maintaining a hot environment for buildings and people. UHI has a significant impact on heat stress, thermal comfort and energy demand of the buildings and people in urban areas. Therefore, it is important to consider it in building design and simulations (Manoli et al. 2019).

This study uses Urban Weather Generator (UWG) method to project the influence of UHI effect on typical future weather data and observed weather data. UWG is a methodology and software tool that estimates hourly urban canopy air temperature and humidity ratio based on urban morphological parameters and urban land use (Bueno et al. 2013). It can be used alone or in conjunction with other existing programs to account for the impact of UHIs.

UWG model contains four interacting components: Rural Station Model (RSM) which estimates sensible heat fluxes; Vertical Diffusion Model (VDM) that calculates vertical air temperature profiles at a rural weather station; Urban Boundary Layer (UBL) that accounts for vertical histograms of the air temperature above the urban coverage; and Urban Canopy and Building Energy Model (UC-BEM) that allows taking into consideration temperature and humidity ratio of the air in the urban canyon (Bueno et al. 2013; Kamal et al. 2021). UWG has previously been validated in several studies for Basel, Singapore, Toulouse, Rome, Barcelona, and Abu Dhabi (Bande et al. 2019).

1.3 Future climate and buildings

Comprehensive time-activity studies in Europe and US have shown that people on average spend 16 hours/day indoors. This number increases to approximately 20 hours/day for those above 64 years old (Brasche and Bischof 2005), asserting the importance of indoor air quality and indoor thermal conditions.

Projected variations in extreme weather events and global temperature increase will further add pressure on buildings, making them uncomfortable or even potentially dangerous to occupants' wellbeing (Green et al. 2016; Hamdy et al. 2017; Yang et al. 2019). Heatwaves in particular can cause severe overheating in buildings that are not equipped to cope with it. It could lead to several problems ranging from thermal discomfort and productivity reduction to illnesses and even death of occupants (Hamdy et al. 2017).

Furthermore, recent buildings have been designed to answer to past climate conditions and often with typical meteorological year (TMY) weather files that are obtained by means and thus do not include heatwaves (Lauzet et al. 2018) or heat island effect. Moreover, past construction regulations and most of the current ones in western and northern Europe are not focused on summer conditions and as a result, even recent buildings can already be highly uncomfortable during the heatwaves (Lomas and Porritt 2017; R. Mitchell and Natarajan 2019; Petrou et al. 2019).

The magnitude of occupant vulnerability inside the building due to overheating depends on several parameters such as duration and intensity of exposure to heat, as well as, on personal adaptation capacity of the occupant. Installation of cooling systems in the already energy-intensive building sector could mitigate associated risks. However, the resulting increase in energy demand would affect global climate change. Moreover, if installed in every household, these systems would dramatically increase the electricity demand for cooling at peak time and at the same time discharge hot air that will further intensify urban warming.

Another factor that affects occupants' vulnerability to future climate conditions and heatwaves is energy precariousness (Battersby 2016). This is especially relevant for naturally ventilated buildings that have traditionally not relied on energy to keep occupants safe from overheating during summer.

For practitioners in the thermal evaluation of buildings, this means that typical weather files created from historical records collected from rural weather stations may no longer be suitable to assess buildings' resilience in the context of future climate and heatwaves.

1.4 Indoor overheating assessment indices

Indoor overheating, similar to thermal comfort, is a dynamic phenomenon that varies both spatially and temporally. Researchers over the years have proposed numerous methods to describe indoor overheating, but still, there is no consensus on how to evaluate it through simulation or measurement (Lomas and Porritt 2017). Therefore, there is a need to specify what we mean by overheating or heat stress in buildings. A literature review on indoor overheating indices by Epstein et al. collected and analysed more than 40 different heat stress indices (Epstein and Moran 2006). Authors argue that too much emphasis has been placed on the academic accuracy of many of these indices at the expense of practicality. They recommend using simple and easy to use indices. Their literature review covered indices that were in use or proposed until 2005. Since then indoor overheating and comfort measurement indices have evolved and a number of new indices have been introduced. The most important change in that front is probably the adoption of adaptive comfort indices by ANSI/ASHRAE Standard 55 and ISSO 74 (Dutch Guidelines) in 2004 and 2005. European standard adopted it in 2007 in EN 15251-1. Adaptive indices were slightly modified and updated in ANSI/ASHRAE Standard 55 in 2017, and EN 16978-1 was introduced in 2019 to replace EN 15251. A review of indices by (Carlucci and Pagliano 2012) proposes to classify

homogeneous indices into four families: (1) percentage indices that demonstrate comfort as a percentage [of time] inside a range such as PMV and CIBSE guidelines; (2) cumulative indices such as degree-hour criterion in EN 15251, and exceedance metrics illustrated by (Borgeson and Brager 2011); (3) risk indices such as Nicol et al.'s overheating risk (J. Fergus Nicol et al. 2009) that suggests thermal discomfort is related to the difference between operative temperature and EN adaptive thresholds, and Robinson and Hadi's overheating risk index (Robinson and Haldi 2008) which is based on the analogy that (the storage) of human tolerance to overheating stimuli may be equivalent to storage of charge in an electrical capacitor, and proposes a simple mathematical model to predict overheating risk given a set of measured environmental conditions; (4) averaging indices such as the average predicted percentage of dissatisfied (PPD), and the difference between peak temperature and annual average. A more recent review on time-integrated overheating evaluation methods for temperate climate regions by Rahif, Amaripadath, and Attia (Rahif, Amaripadath, and Attia 2021) state that most standards recommend using adaptive comfort methods in the assessment of indoor thermal conditions for free-floating buildings, and static approaches for air-conditioned buildings. Their review analyzes 11 international standards, 5 national building codes, and a number of scientific literature that present overheating indices for temperate climate regions. The large number of indices in the literature and national standards indicate that researchers are trying to quantify the relation between human body and climatic stress in a single formula or by a single index. It is, however, obvious that there is a complex relation between the two and using a single index could mask or even exaggerate the indoor thermal conditions. Using multiple indices could probably better explain this relationship because some indices give complementary results and highlight certain aspect of occupants' sensation that are ignored or given less attention by other indices.

In this study, we used three easy to use indices to describe what constitutes indoor over-temperature in a naturally ventilated building.

1.5 Weather data for Building Performance Simulations (BPS)

Three methods of thermal simulations are commonly used nowadays for building performance evaluations: static, semi-dynamic, and dynamic. Of the three, the dynamic method is considered more appropriate in building thermal assessment. This method requires at least hourly weather data that contains temperature, humidity, radiation, wind, atmospheric pressure, etc. Depending on the objective of dynamic BPS, two distinctive weather data types are used: synthetized and observed data. The latter is often used in the performance monitoring phase and is collected from weather stations or by in-situ measurements. The former is more frequently used in the design phase and is synthetically generated from climate normals. WMO defines climate normals as a period that covers at least 30 years of data. For evaluation of buildings' climate resilience, future weather data are required. These data are based on future emission scenarios and projections produced using climate models. Emission scenarios are used as input for General Circulations Models also referred to as Global Climate Models (GCMs). GCMs cover the entire surface of the globe and their spatial resolution is coarse, typically between 150 to 600 km (P.Tootkaboni et al. 2021). Application of given GCMs for building thermal evaluation requires downscaling to a finer spatial and temporal resolution to consider regional and local scale estimates of climate variability and change. As can be seen in Figure 1, there are two main approaches to downscale GCMs: Dynamical downscaling (DDS) and empirical-statistical downscaling (ESD).

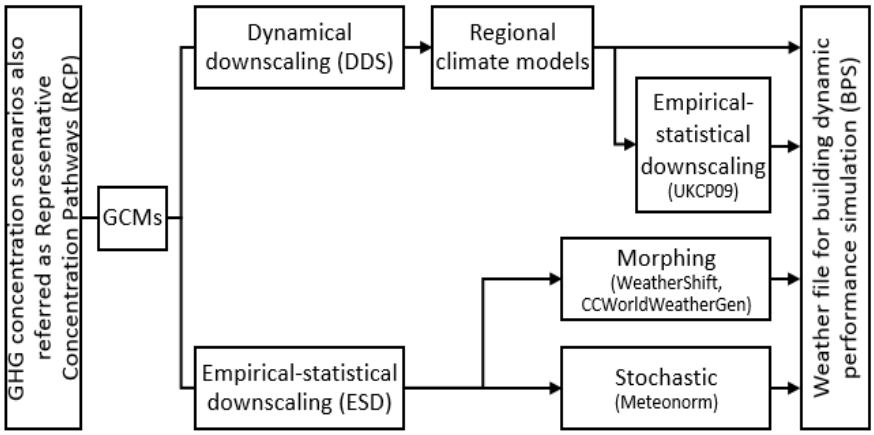

Figure 1: downscaling approaches

DDS and ESD stand on two distinctive philosophies: DDS relies on climate data that are based on our knowledge of physical processes (solving equations for humidity, temperature, local wind, etc.) and ESD makes use of information obtained from the statistical analysis (e.g. regression relationships) of previously observed climate data.

Erlandsen et al. and Moazami et al. (Erlandsen et al. 2020; Moazami et al. 2019) in their studies have also discussed a hybrid approach in which the results of dynamically downscaled GCMs, also referred to as Regional climate model (RCM), stored at a coarse resolution undergo further downscaling using statistical approach.

Several studies have been conducted on the relative difference of DDS and ESD on climate impact assessments. P.Tootkabani et al. (P.Tootkaboni et al. 2021) in their paper on comparative analysis of different future weather data for building energy simulations, compared weather files from three tools that are based on ESD (WeatherShift, Meteonorm, and CCWorldWeatherGen) with one DDS future typical meteorological year. Their results show that all ESD weather files have relatively similar operation in predicting thermal comfort and energy consumption in buildings in comparison to DDS weather files. Their paper also states that the ESD method, regardless of how it is used can provide sufficient information to perform comparative analysis on long-term variations in energy consumption of buildings, but existing inconsistency within the method can lead to significant prediction

error. Under such conditions, they found the DDS method more reliable when the objective of the study is to investigate and communicate the resilience of buildings to future climate conditions. Ramon et al. (Ramon et al. 2019) in their paper state that ESD method is more suited to investigate average energy performance in future climate realization but less suited to assess extreme conditions. DDS, on the other hand, can be used for both average and extreme assessment purposes. Moazami et al. (Moazami et al. 2019) in their study on the impact of future weather data types on building energy performance concluded that weather files generated using DDS that take into account both typical and extreme climatic conditions are most reliable to evaluate energy robustness in the context of future climate uncertainties. In the present study, availability of open-source RCMs (dynamically downscaled GCM) data from EURO-CORDEX presented an opportunity to systematically compare three future DDS climate models and one future ESD model, assuming the high-emission scenario [representative concentration pathway (RCP) 8.5], with observed weather data of 2003. The latter was accessed from MeteoFrance archives and transformed into EnergyPlus (.epw) file format that can be used in BPS.

The aim of this study is, first, to provide insights for practitioners in BPS on how to generate future and present ready-to-use weather files using open-source RCMs, and second, through a comparative analysis with heatwave weather data of 2003 show their potential in indoor overheating assessment of buildings' considering urban heat island effect. The method described here does not illustrate in detail the uncertainties associated with emission scenarios, climate projections, climate models, and bias adjustment of climate models as they were addressed previously by (Hosseini, Bigtashi, and Lee 2021; Machard et al. 2020; Maraun 2016).

The method/workflow to generate typical weather files is of particular interest for practitioners in building simulations that use current or future weather data in thermal

performance evaluation of buildings. Implementation of the approach we used to compare and evaluate indoor overheating of two free-floating buildings with two weather files and three indices contribute to the existing body of knowledge in the assessment and study of climate-change-proof buildings.

The next section of this document, materials and methods, is structured as follows: first sub-section describes the workflow to extract yearly weather data for any location; second sub-section demonstrates the methodology to assemble typical weather file from downloaded yearly data; third sub-section presents the method used in comparative analysis of weather files; fourth sub-section depicts the application of weather files on two buildings case study. The final section summarizes and discusses the results, limitations and prospects.

2 Materials and Methods

2.1 Extracting yearly weather data

Coordinated Regional climate Downscaling Experiment CORDEX (www.cordex.org) is an international coordinated effort supported by World Climate Research Programme's Working Group on Regional Climate. As a part of CORDEX, EURO-CORDEX is today the main reference framework for regional downscaling research of climate data. The main goals of this experiment are: (1) to evaluate and improve different RCMs, (2) to better understand regional and local climate phenomena through downscaling, (3) to generate coordinated RCM projections at the global scale, (4) and enable users of regional climate data to exchange knowledge (Daniela et al. 2020).

EURO-CORDEX maintains a consistent database of multi-year historical and projected data that can be used for climate adaptation studies in various sectors. The data for Europe is available on a horizontal grid resolution of 0.11° x 0.11°, equivalent of 12.5 km (Jacob et al. 2014). All necessary components to generate weather files for building

simulations can be downloaded at 3h, 6h, daily, monthly and seasonal temporal resolution. For this study, we downloaded 3h time-step data.

In this study, EURO-CORDEX regional climate projection data were accessed via the Climate Data Store (CDS) portal supported by the Copernicus Climate Change Service (C3S) initiative that provides information about past, present, and future climate in Europe and the rest of the world[1]. CDS portal allows accessing climate variables of GCMs and RCMs in various combinations and different horizontal and temporal resolutions. Raw data is available in NetCDF (Network Common Data Form) file format that is commonly used within the climate modelling community to share array-oriented scientific data. Climate data in this format are stored in multi-dimensions and users can view/access geographical coordinates (latitude, longitude), time, level, climate variable (temperature, relative humidity, etc.). Practitioners are cautioned to check for bias-adjustment of climate data before using them in BPS. In this study, raw data were downloaded from the CDS portal and they are not bias adjusted.

Figure 2 depicts the near-surface air temperature of an RCM in EURO-CORDEX region as well as the position of our case study city (Nantes) in a NetCDF file.

lev

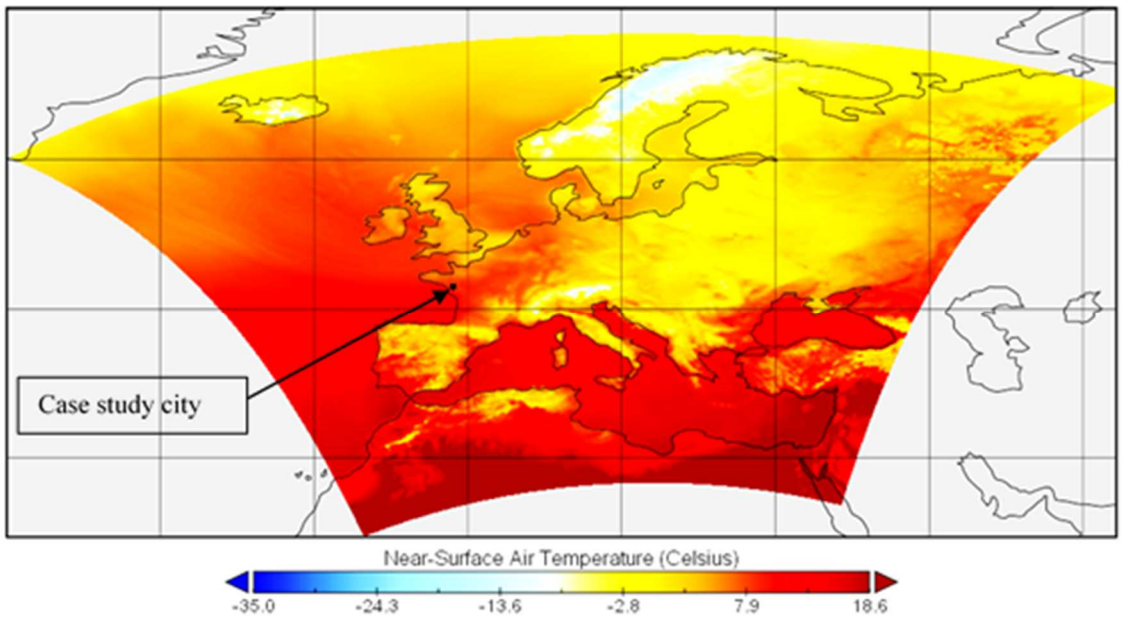

Figure 2: Near surface air temperature NetCDF data file visualized in Panoply

Data of Nantes were extracted using a python script that identified the closest point of the data grid in the NetCDF file to the assigned latitude and longitude coordinates.

Six climate variables (dry-bulb temperature [K], relative humidity [%], global solar irradiance [W/m^2], cloud cover [%], atmospheric pressure [Pa], and wind speed [m/s]) as suggested by (Machard et al. 2020) were downloaded for thirty years (2040 to 2070) of the following global-regional climate models:

Table 1: dynamically downscaled climate models

	Institution	Global climate model (GCM)	Regional climate model (RCM)	GCM_RCM names used
1	CNRM	CNRM-CERFACS-CM5 (France)	CNRM-ALADIN63 (France)	CNRM_ALADIN
2	SMHI	IPSL-CM5A-MR (France)	SMHI-RCA4 (Sweden)	ISPL_SMHI
3	GERICS	MPI-M-MPI-ESM-LR (Germany)	GERICS-REMO2015 (Germany)	MPI_REMO

The climate models in Table 1 were chosen based on the availability of completed simulations with all six climate variables for RCP8.5 scenario experiments at 3h time-step interval. More combinations of GCM and RCM are possible in the CDS portal but, here, we only used each GCM and RCM once.

Dry-bulb temperature was first converted from Kelvin to degrees Celsius. Polynomial interpolation (n=7) was used to convert 3h time-step data to 1h time-step for dry-bulb temperature and global solar irradiance and linear interpolation for the rest of the variables.

Dew point temperature (T_d) was estimated from dry bulb temperature and relative humidity using August–Roche–Magnus formula for dew point temperature approximation (Thiis et al. 2017).

$$T_d = \frac{b[ln\left(\frac{RH}{100}\right) + \frac{a \cdot T}{b+T}]}{a - ln\left(\frac{RH}{100}\right) - \frac{a \cdot T}{b+T}}$$

Where: RH Relative humidity [%]

T Dry bulb temperature [°C]

a = 17.27, b = 237.7 °C, for T ≤ 60 °C and an error of ±0.4 °C.

Sunrise and sunset time for the given location was calculated using Python Astral package, which is based on equations from Astronomical Algorithms, by Jean Meeus. Interpolated global solar irradiance data that were before sunrise and after sunset were set to zero. Solar zenith angle, direct normal irradiance, and diffuse horizontal irradiance were calculated following the methodology described by (Machard et al. 2020). Following the steps described above, for each year of each climate model, a yearly weather file was generated. In the next step, 30 years of weather data for each climate model were assembled to generate future typical weather files.

2.2 Assembling typical weather files

We used EN ISO 15927-4 2005 standard created by the European Committee for Standardization, proposing a method for constructing reference year of hourly weather data to generate typical future weather file. In this method, dry-bulb temperature, relative humidity, and global horizontal irradiance climate variables are the key parameters in the selection of "best" months to form reference year, with wind speed as a secondary (ISO 15927-4 2005).

Following the ISO 15927-4 method for each climate model, we first merged 30 years of hourly weather data and calculated daily means. Then for each calendar month, cumulative distribution function (CDF) of daily means of every year and of multiple-year were calculated.

For each calendar month, Finkelstein-Schafer statistic (FS) was calculated and individual months from the multiple-year dataset were ranked in ascending order.

For each calendar month and each year, separate ranks were added for each of the three key parameters. ISO 15927-4 gives equal weighting to three key climate parameters. Therefore, ranks of key parameters were only added to one another and ranked in ascending order. Of the three months with lowest total ranking for three key parameters, the one with the smallest wind speed deviation was selected as the "best" month to be included in the reference year. After identification of "best" month for each month from multiyear data, they were joined together to form a reference year. In order to smooth the transition from one month to another, eight hours at the end and beginning of subsequent months were interpolated, including last eight hours of December and first eight hours of January. The procedure is also presented in Figure 3.

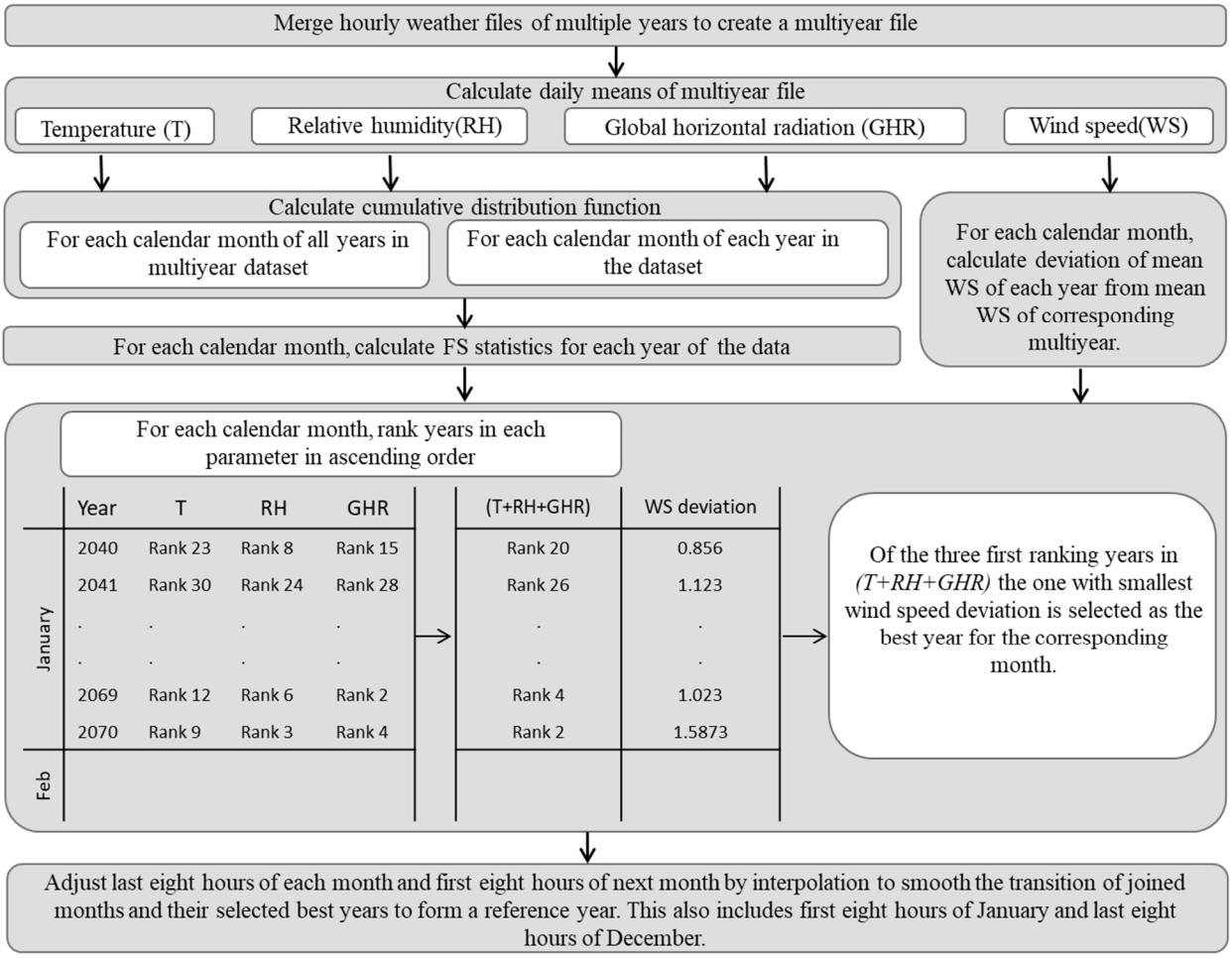

Figure 3: Workflow to assemble typical weather file

As an example, Figure 4 shows cumulative distribution function plots of dry-bulb temperature, relative humidity, global horizontal irradiance and mean wind speed deviation plot for the calendar month of July in the IPSL-SMHI model. In this example, from the three key parameters, July of 2050, July of 2060 and July of 2061 were candidates of the best month for reference year. Among them, July of 2061 had the smallest wind speed deviation from July in the multiyear dataset. Therefore, it was selected as the "best" month for the reference year.

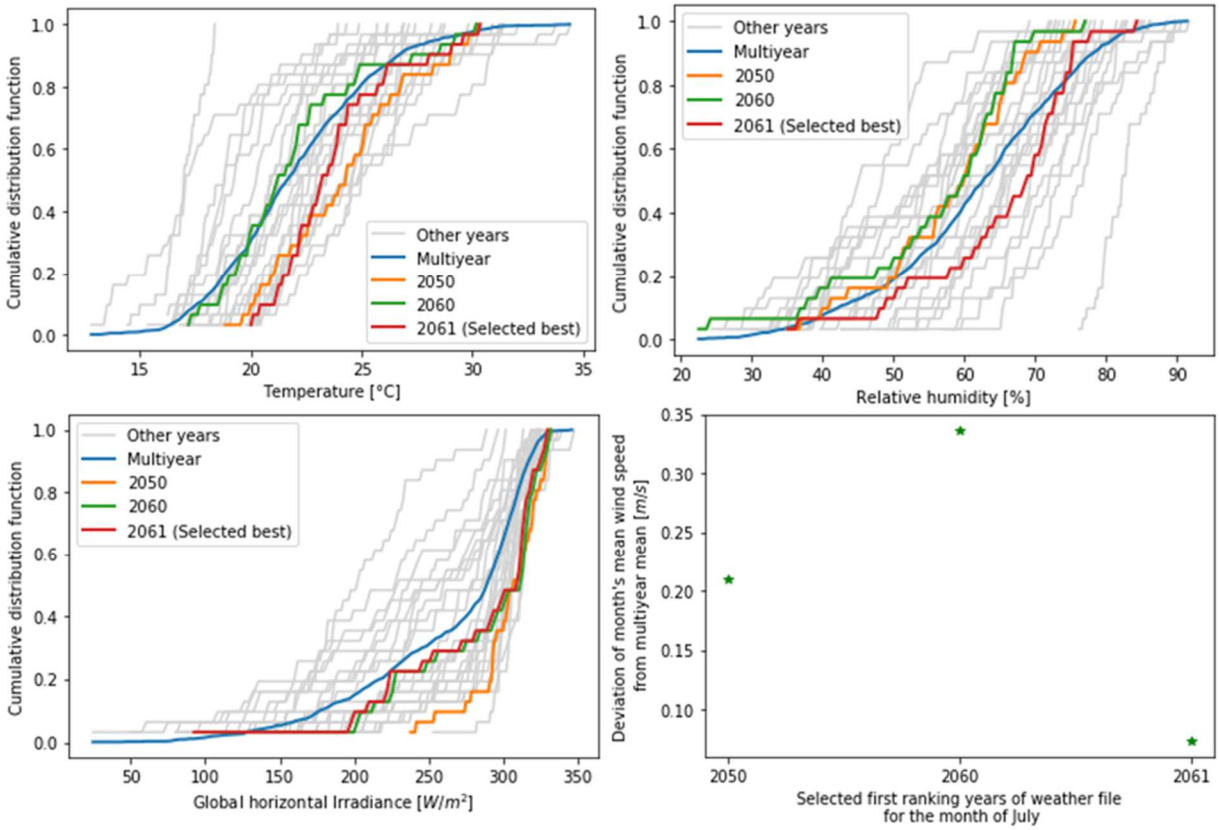

Figure 4: CDF plots of three key parameters and plot of wind speed deviation for July calendar month in IPSL-SMHI climate model

Using the method described, three future typical weather files (2040 to 2070) for the case study city from dynamically downscaled climate models were assembled.

For comparative analysis, observed weather data of 2003, and one ESD future weather scenario (Meteonorm RCP 8.5 2050) was also downloaded from MeteoFrance archives and Meteonorm v.8 software respectively, for our case study city, Nantes.

2.3 Comparative analysis of weather files

Statistical distribution of monthly dry bulb temperature, relative humidity, and global horizontal irradiance of each DDS climate model, as well as Meteonorm RCP 8.5 2050, and measured weather data of 2003 were compared. Additionally, heating degree-days (HDD) and cooling degree-days (CDD) indices in each weather file were calculated using the methodology and base temperatures recommended by EUROSTAT to form a common and comparable basis in comparison. These two indicators are commonly used to give a rough estimation of heating and cooling energy demand. Calculation of HDD and CDD both rely on base temperature, which depends in principle on various factors related to building and surrounding. In this study, base temperature in HDD calculation was set to constant value of 15°C and in CDD calculation to 24°C. In HDD calculation, if $T_m \leq 15°C$ then HDD = $\sum_i(18°C - T^i_m)$, else HDD = 0, where T^i_m is the mean air temperature of day i.

Similarly in calculation of CDD, if $T_m \geq 24°C$ then CDD = $\sum_i(T^i_m - 21°C)$, else CDD = 0 (Bhatnagar, Mathur, and Garg 2018).

Weather files were also investigated with a temperature-based index to check the frequency and intensity of heatwaves in them. This temperature-based heatwave index was developed for France after the exceptional heatwave in the summer of 2003. This index relies on the heatwave and health alert system (Sacs) piloted by Public Health France. The objective of it is to anticipate heat waves that are likely to have a major health impact. Every day, in each metropolitan department, the level of risk is assessed by MeteoFrance comparing forecasts of meteorological indicators with departmental alert thresholds. Thresholds are shown in Figure 5, below.

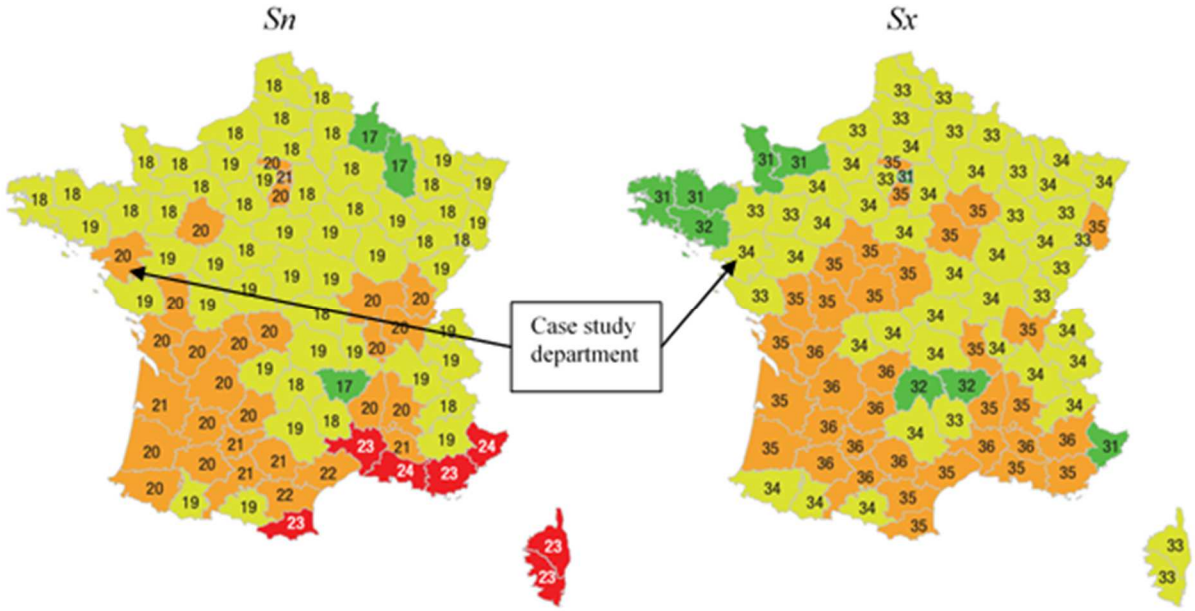

*Figure 3: Heatwave meteorological indicator thresholds, **Sn**: threshold for the three-day average of minimum temperatures in [°C]. **Sx**: threshold for the three-day average of maximum temperatures in [°C].*

These thresholds are defined on the basis of a historical analysis and with an aim to anticipate heat waves that are likely to be associated with excess mortality of at least 50% in 4 major cities and 100% in smaller cities. In this method, "*A heatwave is defined as a period when the minimum and maximum temperatures, averaged over three days, simultaneously reach or exceed departmental alert thresholds*". The onset of a heatwave corresponds to the first day on which the meteorological indicators of Sacs (average over three consecutive days of minimum and maximum temperatures) reaches or exceeds alert thresholds (Figure 5). The end of a heatwave is the last day of meeting or exceeding these thresholds (Wagner, 2006). The Sacs thresholds have seen certain evolutions over the years and the threshold presented in Figure 5 are those of 2016. Selected weather files for the case study city were measured against the heatwave meteorological thresholds of the case study city department. To do so, maximum daily temperatures (IBM_max) and minimum daily temperature (IBM_min) of weather files were extracted from hourly data. A python script was written to detect and measure the heatwaves parameters such as start date, duration, peak temperature, intensity of maximum temperatures, and intensity of minimum temperatures.

2.4 Application of weather data on two residential buildings

One single-family house (SFH) and one multifamily house (MFH), located in Nantes city, were used to carry out comparative analysis of weather data by assessing hourly indoor thermal conditions of five summer months (May, June, July, August, September). The two buildings were selected after a typological analysis of residential building stock and these two were identified as representative of two types of residential buildings in Nantes city. MFH was located in a densely built part of the city, where building footprint density is 53%, and SFH was located in a more sparsely built neighbourhood, where buildings covered 18% of the land surface in a 200-meter radius (Figure 6).

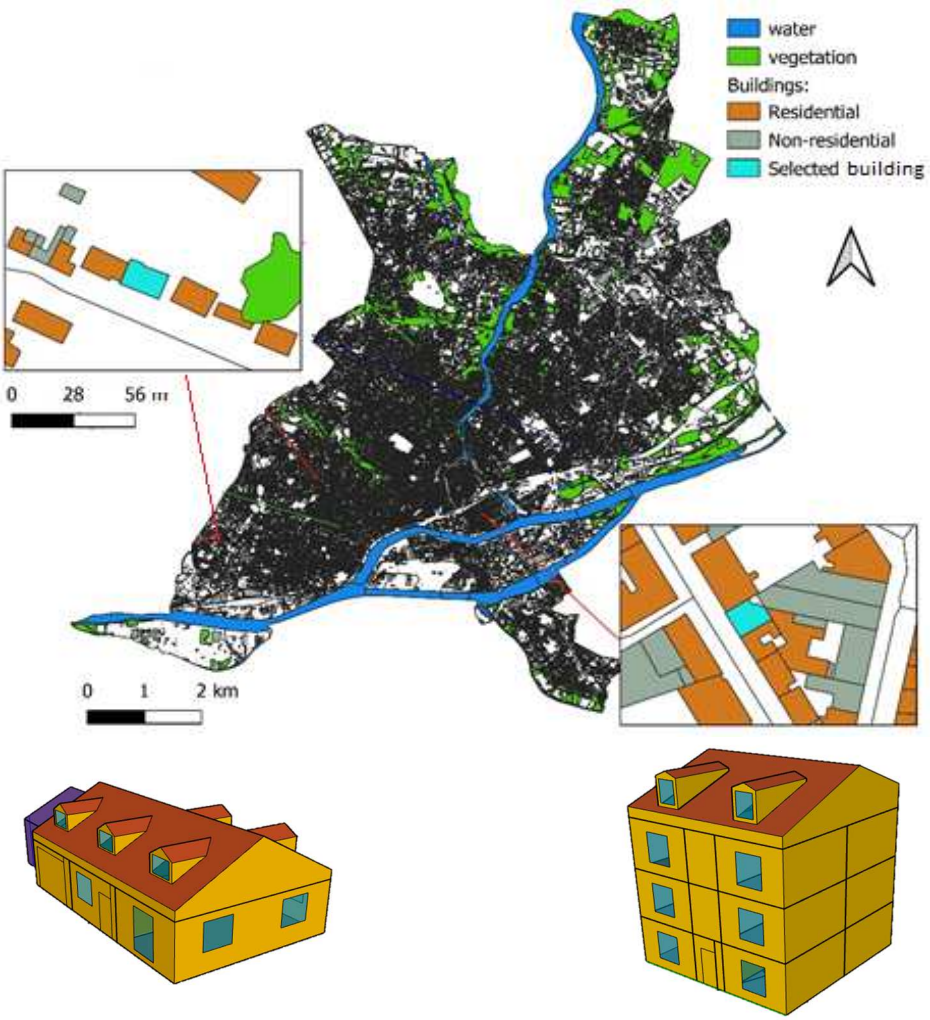

Figure 4: The two studied buildings (down), and their location in the city (up)

SFH built in 1981 has insulated envelop components as it was constructed after the first French law on energy saving. MFH has uninsulated envelope elements because it was constructed before the introduction of the first French law on energy saving. Both buildings are connected to a central heating system for winter heating but they do not have mechanical cooling mechanism. Table 2 contains estimated thermo-physical properties of envelop elements for the selected buildings. Thermo-physical parameters of the buildings were estimated as a function of their year of construction from the article of Civel and Elbeze (Civel and Elbeze, 2016).

Table 2: Thermo-physical properties of envelop elements

#	Envelope element	U value [W/m²K]	
		SFH	MFH
1	Exterior wall	0.8	2.42
2	Exterior roof	0.5	2.3
3	Window	2.8	2.9
4	Adjacent walls	2	2
5	Adjacent roof/ceiling	3	3
6	Orientation of main facades	North-South	East-west

Heat gains from lighting load both in SFH and MFH was estimated to be 10 W/m^2. Density of occupants was set according to EN 16798-1 to 42.5 m^2/person and 28.3 m^2/person in SFH and MFH respectively. Occupancy schedule for both SFH and MFH is presented in Figure 7.

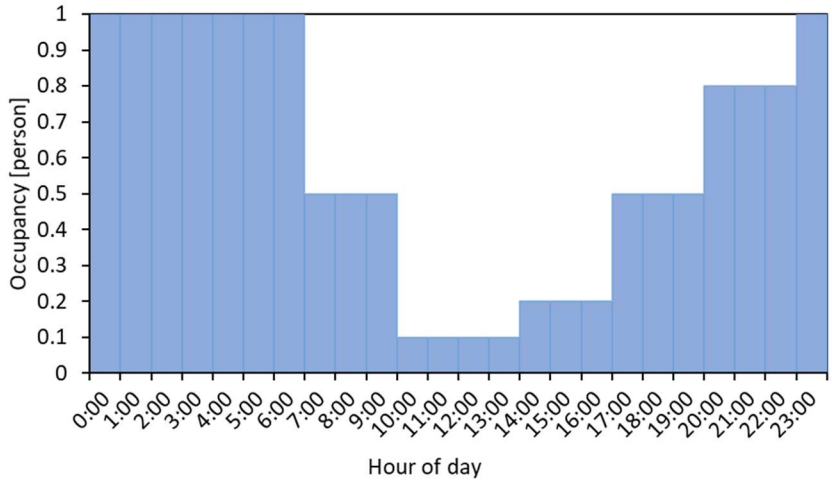

Figure 7: Occupancy schedule according to EN 16798 -1

Occupants of both buildings are assumed to be highly conscious of their environment and would adjust natural air inflow and shading for better comfort. During five summer months, occupants would open the windows every day 2 hours in the morning and 5 hours in the evening, which is approximately 29% of the day. Air inflow rate to each zone was assumed 0.7 ACH when openings/windows were closed or there was no window in the zone. It was assumed 1.3 ACH if there is one opening in a thermal zone and its status is open. For two or more openings in a thermal zone, air inflow rate was assumed 1.9 ACH when its status

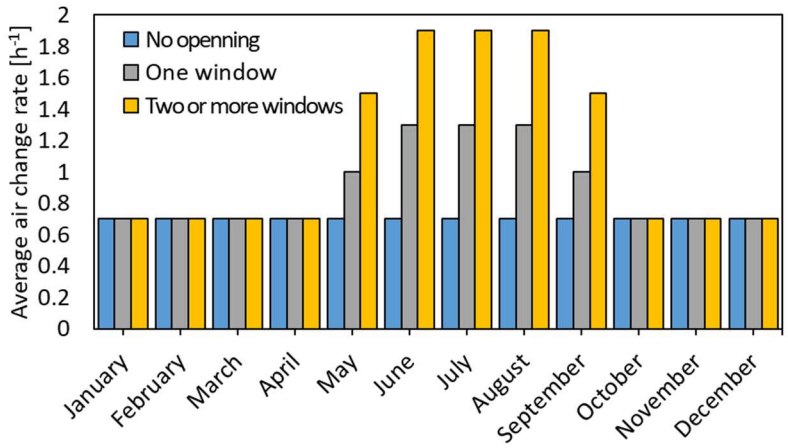

Figure 5 : Modelled infiltration rate into different thermal zones

is open. (Figure 8).

Windows in SFH and MFH, both were equipped with manual roller blinders/shutters allowing occupants to control direct solar radiation intake into the zones. In the summer months, during the day, occupants were assumed to use external shadings to cover 60% of the area of window and during the night 50% of the area (Figure 9).

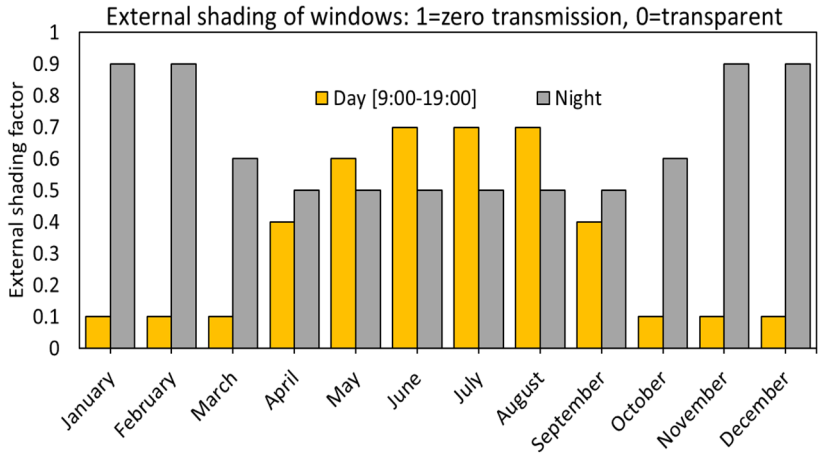

2.5 Considering urban heat island effect

UWG Python package was used to project the influence of UHI effect on the weather files. Main input of UWG is the rural weather file, also referred to as baseline weather file, in EnergyPlus (.epw) file format. Other input parameters are climate zone/location of the city, building typology distribution, urban parameters, and building parameters. UWG model allows practitioners to add detailed information about buildings and its surrounding, but (Salvati, Palme, and Inostroza 2017) in their paper on key parameters for urban heat island assessment in a Mediterranean context, suggest that urban morphological parameters have the highest effect on UHI intensity and therefore can be used as descriptors of urban climatic performance in various urban areas.

In this study, urban morphological input parameters for UWG model were calculated within the 200-meter radius of each building. Both SFH and MFH were located in the same city, therefore had the same climate zone, 4A. Approximately 60% of buildings within the 200-meters radius of MFH were multifamily residential buildings and the rest were non-residential buildings. Almost 80% of buildings located within the 200-meter buffer radius of SFH were residential buildings, both single family and multiple family houses. Within the 200-meters radius, building footprint density, average height, tree coverage ratio, green coverage rate, ratio of vertical surfaces to horizontal surfaces, and year of construction were estimated for SFH and MFH separately. These parameters were used as input for the UWG model to modify weather files for the urban heat island effect.

Urban morphological parameters listed above for each building, within the assigned radius, were accessed and calculated from BDTOPO database. BDTOPO is a 2D and 3D vector spatial database containing the description of landscape elements including but not limited to building footprint, building height, building year of construction, vegetation coverage, water coverage ratio, presence of trees, transportation routes, etcetera throughout France.

Two baseline weather files (2003 observed weather data & IPSL-SMHI 2040-2070) were modified using UWG model for SFH and MFH separately. Monthly average temperatures differences between baseline and modified weather files were calculated for both buildings. The differences calculated show the average monthly intensity of UHI effect projected on the baseline weather file by UWG model.

2.6 Indoor overheating assessment indices

In this study, we employed three widely used indoor overheating indices to measure summer performance of buildings: EN 16798-1 adaptive comfort index, Givoni bioclimatic index, and constant temperature of 27 °C. These three indices were selected to check if the impact of the weather file employed also depends on the way results are exploited.

Adaptive comfort index is based on the idea that control over the immediate environment allows occupants to adapt to a wider range of thermal conditions. With reference to this principle, EN 16798-1 norm for adaptive comfort is related to exponentially decaying weighted mean outdoor temperature (T_{RM}).

$$T_{RM} = (1-\alpha)\,[T_{N-1} + \alpha\, T_{N-2} + \alpha^2\, T_{N-3} + \alpha^3\, T_{N-4} + \alpha^4\, T_{N-5} + \ldots]\ (^{\circ}C)$$

Where: α Constant between 0 and 1

T_{N-n} Mean outdoor daily temperature for *n* days prior to target day

In the calculation of weighted mean outdoor temperature, α constant controls the speed of changes in running mean outdoor temperature. Based on Smart Controls and Thermal Comfort (SCATs) project recommended value for it is 0.8 (McCartney and Fergus Nicol 2002). Standard also recommends that prevailing mean outdoor temperature shall be based on no fewer than seven sequential days prior to target day. EN 16798-1 norm for adaptive thermal comfort index illustrates indoor thermal comfort from operative temperatures in three categories: category I, II, III (EN 16798-1 2019).

Category I is considered more suitable for high demanding comfort levels, category II for typical situations and category III for low demanding levels.

Following equations calculate maximum and minimum allowable indoor operative temperature limits (T_{MAX} & T_{MIN}) when 10 ºC < T_{RM} < 30 ºC.

Category I	Upper limit:	T_{MAX} (ºC) =0.31*T_{RM} + 18.8 + 2
	Lower limit:	T_{MIN} (ºC) =0.31*T_{RM} + 18.8 - 3
Category II	Upper limit:	T_{MAX} (ºC) =0.31*T_{RM} + 18.8 + 3
	Lower limit:	T_{MIN} (ºC) =0.31*T_{RM} + 18.8 - 4
Category III	Upper limit:	T_{MAX} (ºC) =0.31*T_{RM} + 18.8 + 4
	Lower limit:	T_{MIN} (ºC) =0.31*T_{RM} + 18.8 - 5

Optimal operative temperature in EN 16798-1 equals to:

$$T_{COMFORT}\,(ºC) = 0.31*T_{RM} + 18.8$$

In this study, ***degree-hours*** and ***percentage-of-hours*** indoor operative temperature inside each thermal zone of building exceeding the upper boundary limits in category I, II, and III of EN 16798-1 were calculated.

In Givoni bioclimatic index, as depicted in Figure 10, thermal comfort polygons are

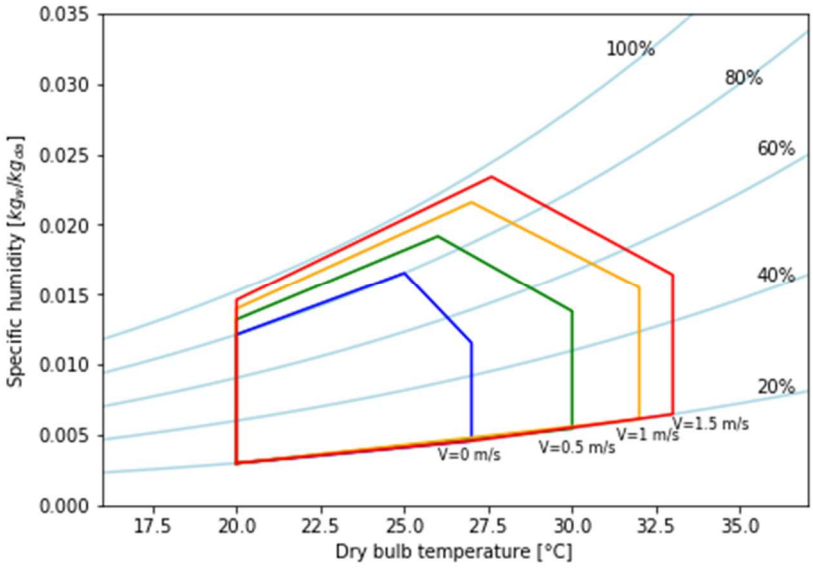

Figure 7: Psychometric chart and Givoni bioclimatic design polygons

presented on a psychometric chart (Malet-Damour 2012).

The lines of polygons, shown above, determine the limits of effectiveness of design strategies for indoor thermal conditions in relation to indoor wind speed for an occupant engaged in sedentary activity and wearing summer clothing (0.5 clo). Psychometric chart lines, on which thermal comfort polygons are drawn, are related to the air pressure. The latter is estimated using barometric formula as a function of height above sea level. Average height of our case study city from sea level is around 30 meters.

$$p = 101325\ (1 - 2.25577 * 10^{-5}\ h)^{5.25588}$$

Where:

h – Average height above sea level

Ideal comfort region with this index is the polygon (v=0 m/s), where air temperature is between 20 to 27°C, relative humidity is between 20 to 80%, and indoor air velocity is 0 m/s. Second polygon is called natural ventilation comfort zone, where indoor air temperature is between 20 to 30°C, relative humidity is between 20 to 90%, and air velocity is up to 0.5 m/s. Air velocity in the third polygon is 1m/s and it is induced both by natural ventilation and ceiling fans. Indoor air temperature in the third polygon is between 20 to 32°C and relative humidity is between 20 to 94%. We added the fourth polygon, where air speed is 1.5 m/s, for extreme cases, because it has been used and considered acceptable in some hot and warm countries (J.F. Nicol 1974). Marginal temperature gain of air velocity increase from 1 m/s to 1.5m/s is less than 1 degree Celsius (Kumar et al. 2019), therefore, the maximum temperature of polygon four (v=1.5 m/s) is 1 degree Celsius higher than polygon three (v=1 m/s).

In comparative analysis, ***number of hours*** that indoor air temperature and relative humidity were within and outside the depicted polygons were calculated for all zones and buildings.

Constant temperature of 27 °C as an index of thermal comfort, in this study, was selected with reference to the night-time temperature threshold of 26 °C proposed by Chartered Institution of Building Services Engineers (CIBSE). According to CIBSE, night-

time indoor temperature should not exceed 26 °C more than 1% of annual hours for occupants to sleep well. Considering the adaptive capacity of occupants, difference between the climate of UK and France, mild relative humidity of our case study city, and the fact that we use this index both during day and night, it was decided to use 27 °C instead of 26°C as the threshold value to measure comfort along with other indices. In comparative analysis, peak indoor temperature and maximum number of consecutive hours that indoor temperature exceeded 27 °C were calculated.

3 Results and Discussions

3.1 Comparative analysis of weather files

The objective of this sub-section is to analyse the differences in various climate models at monthly scale with different climate variables. Monthly statistical distribution of dry bulb temperature, global horizontal irradiance, and relative humidity of three DDS models, one

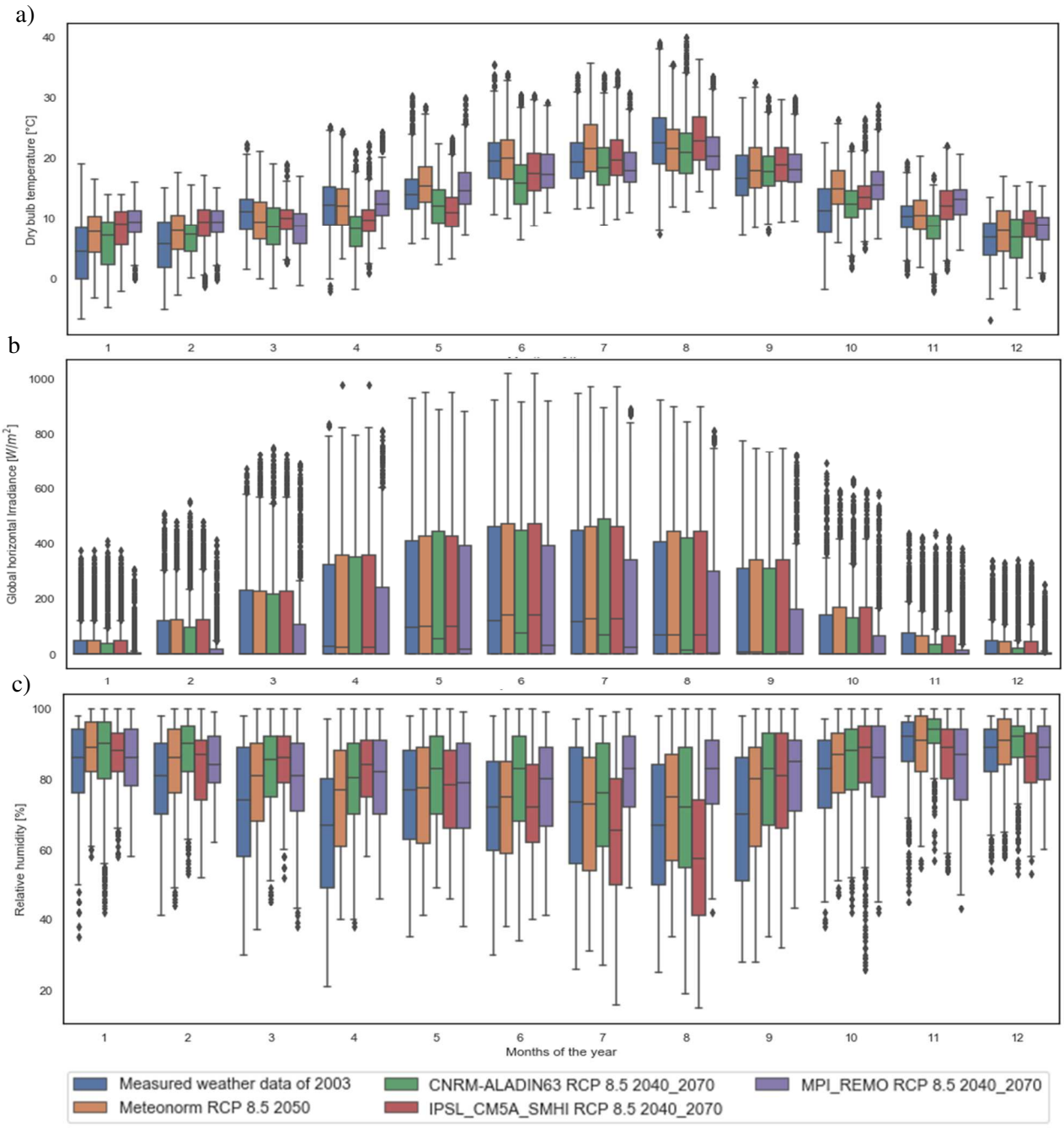

Figure 8: Monthly statistical distribution of: a) dry bulb temperature, b) global horizontal irradiance, c) relative humidity

ESD (meteonorm 2050), and 2003 observed weather data are shown in Figure 11.

Observed weather of 2003 was selected for comparison because it was the severest heatwave recorded in France up until June 28, 2019, when a temperature of 45.9°C was recorded during another heatwave in a weather station in France, exceeding previous record temperature of 2003 by almost 2°C. In contrast to the 2003 heatwave, number of excessive mortality was considerably lower mainly because the duration of 2019 heatwave was shorter and there were better heat-response plans in place (D. Mitchell et al. 2019).

Moving back to comparative analysis, boxplots in Figure 11 show significant variations in monthly mean values among the selected weather data files. This indicates a great difference in predictions from one climate model to another. All three dynamically downscaled weather files and Meteonorm weather file for 2050 show a consistent higher mean monthly value of dry bulb temperature and relative humidity compared to observed weather data of 2003 in winter months. However, the differences in global horizontal irradiance seem insignificant and do not provide enough evidence to notice an upward or downward trend.

Zooming in into summer months, we notice that mean monthly dry bulb temperature in July, August, and September of IPSL-SMHI climate model is closest to mean monthly temperature of 2003 measured weather data. For the same summer months, mean relative humidity of Meteonorm 2050 is closest to 2003 measured weather file.

Among dynamically downscaled weather files, CNRM-ALADIN and MPI-REMO predict higher relative humidity but lower global horizontal irradiance and dry bulb temperature during summer months. IPSL-SMHI, on the other hand, predicts higher temperature and global horizontal irradiance but lower relative humidity for the same summer months. Comparing the length of whiskers and size of interquartile ranges in boxplots for dry bulb temperature and relative humidity variables show that Meteonorm 2050, MPI-REMO, and IPSL-SMHI weather files have relatively smaller dispersion compared to measured

weather data of 2003 and CNRM-ALADIN weather files, in most months of the year. The dispersion is better visible in the month of August when the heatwave of 2003 occurred. This could indicate that measured weather of 2003 and CNRM-ALADIN contain more severe temperature anomalies compared to other climate models investigated here. Variations in weather files are also reflected in the number of HDD and CDD, presented in Table 3.

Table 3: Number of Heating Degree Days (HDD) and Cooling Degree Days (CDD) in different climate models for case study city

#	Base temperature for HDD and CDD calculation [°C]	Observed data	Statistically downscaled	Dynamically downscaled FTWY		
		Measured weather data of 2003	Meteonorm RCP 8.5 2050	CNRM-ALADIN RCP 8.5 2040-2070	IPSL_SMHI RCP 8.5 2040-2070	MPI_REMO RCP 8.5 2040-2070
HDD	15	2106	1741	2365	1873	1595
CDD	24	103	86	62	67	26

Main purpose of HDD and CDD is to demonstrate heating or cooling energy demand of buildings. The spike in CDD for observed weather data of 2003 is most likely due to heatwave data for the month of August in the weather file. Spike in HDD in CNRM-ALADIN, on the other hand, is probably due to a cold snap in March and April, shown in (Figure 11, a). Application of heatwave presence assessment index, described in section 2.3, also detects heatwave that is likely to have major health impact only in CNRM-ALADIN typical future weather data and measured weather file of 2003 (Figure 12).

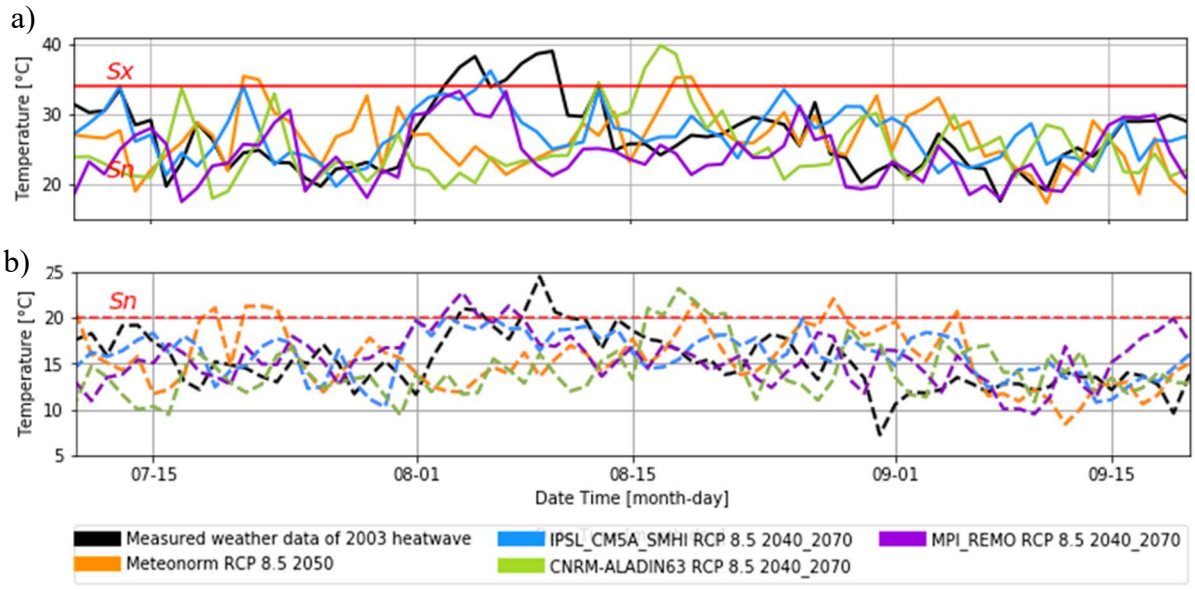

Figure 9: a) Maximum and, b) minimum daily temperatures of weather files plotted alongside heatwave meteorological indicator thresholds

In Figure 12, red straight lines show the position of heatwave thresholds, colours represent weather files, solid lines demonstrate maximum daily temperatures, and dashed lines indicate minimum daily temperatures.

Duration of heatwave detected in CNRM-ALADIN weather file is 3 days and peak temperature is 39.9 degrees. In 2003 measured weather data, the duration of heatwave is 9 days and peak temperature reaches up to 39.1 degrees.

The absence of major heatwave in IPSL-SMHI, Meteonorm, and MPI-REMO could be due to two reasons: first, future weather files generated with this methodology selected the most typical months of the medium future scenario that do not contain extreme weather scenarios and second, the thresholds specified by the definition of heatwave for this administrative department are too high. For instance, maximum consecutive peak daily temperature threshold for Paris is 33°C but for our case study city, it is 34 °C. The definition of heatwaves used here only quantifies the health and mortality impact of the most serious historical events, but not the total impact of heat. Since a moderate temperature increase also has an impact if it persists for an extended period, we think in the future studies of heatwaves in this administrative department, when the focus is more than just health implications, then a

different heatwave definition could be used, such as upper tail percentile approach described by Raei et al. (Raei et al. 2018).

In this study, weather data of heatwave in 2003 and CNRM-ALADIN future weather file both meet the heatwave thresholds that could lead to excess mortality for our case study city. Therefore, for our case study city, measured weather data of 2003 and CNRM-ALADIN are both suitable to study heatwave impact on indoor overheating during summer months for medium future. However, if the study period also includes winter months, the 2003 measured weather file alone may not be suitable because it underestimates temperature increase due to climate change for winter months. Therefore, 2003 weather file has to be accompanied with a FTWY to obtain results that are more reliable. Due to the absence of a concrete reference for future weather conditions, it is difficult to declare one climate model is better than others; nonetheless, considering monthly statistical dispersion and presence of anomalies we selected measured weather data of 2003 for indoor overheating evaluation of our studied buildings during heatwave and IPSL-SMHI weather file for future climate scenario.

3.2 Urban heat island effect on weather data

Weather files selected in previous section were then modified for urban heat island effect, individually for each studied building, using UWG model before being used in Trnsys v.17 for multi-zone dynamic building simulations. Inputs of UWG model were urban morphological parameters and two baseline weather files (2003 observed weather data and IPSL-SMHI typical future weather file). Outputs of UWG model were new weather files containing urban microclimate data in terms of temperature and relative humidity. The output files were then compared to baseline weather files to evaluate the efficacy of UWG methodology on different weather files. In this comparison, mean monthly temperature of baseline weather file was subtracted from mean monthly temperature of modified weather file. Results of this comparison are presented in Table 4. Differences between baseline and

modified weather files show the intensity of UHI effect projected by UWG model for each studied building as a function of their urban morphological characteristics.

Table 4: Monthly mean UHI effect projected by UWG model for SFH and MFH (°C)

	2003 observed weather data		IPSL SMHI 2040_2070	
	MFH	SFH	MFH	SFH
January	0.67	0.48	0.32	0.19
February	0.78	0.60	0.26	0.17
March	0.84	0.74	0.32	0.22
April	0.94	0.84	0.65	0.52
May	1.01	0.88	0.82	0.68
June	0.97	0.84	0.91	0.81
July	1.04	0.91	0.88	0.77
August	1.88	1.68	0.90	0.76
September	1.64	1.54	1.06	0.94
October	0.79	0.66	0.97	0.87
November	0.44	0.33	0.33	0.24
December	0.48	0.33	0.36	0.26

As can be seen in Table 4, temperature difference between modified and baseline weather files for both buildings is consistently higher in summer compared to winter months. UHI effect projected on MFH is higher than on SFH throughout the year, most likely because it is located in a more densely built area and has a lower ratio of vegetation and greenery. Additionally, UHI effect projected on two weather files by UWG for the same urban morphological parameters varies considerably. To investigate this variation, we compared climate variables of the two weather files and the difference in the magnitude of UHI effect between the two but did not notice any clear correlation between model performance and climate variables. However, temperature, relative humidity, wind speed, global horizontal irradiance, etc. in the two weather files were not identical and the difference between UHI effect projected on two weather files for the same urban morphological parameters indicates that the magnitude of UHI effect projected also depends on the choice of weather station. This is in line with findings reported by (Bueno, Nakano, and Norford 2015).

3.3 Comparing indoor thermal comfort

Hourly indoor thermal conditions for five summer months (May, June, July, August, September) were evaluated using two weather files for each studied building. Main facades of SFH were oriented north-south and main facades of MFH were oriented east-west (Figure 13). In SFH, attic, thermal zone in the middle of the building and one thermal zone in the east side of the building were selected in thermal comfort evaluation, because they were more exposed to external environmental conditions. In MFH, attic, one thermal zone oriented east, one thermal zone oriented west of the first and middle floor were selected for evaluation. Hourly indoor overheating indicators for each thermal zone were calculated after running building performance simulations using the weather files selected and modified in previous sections.

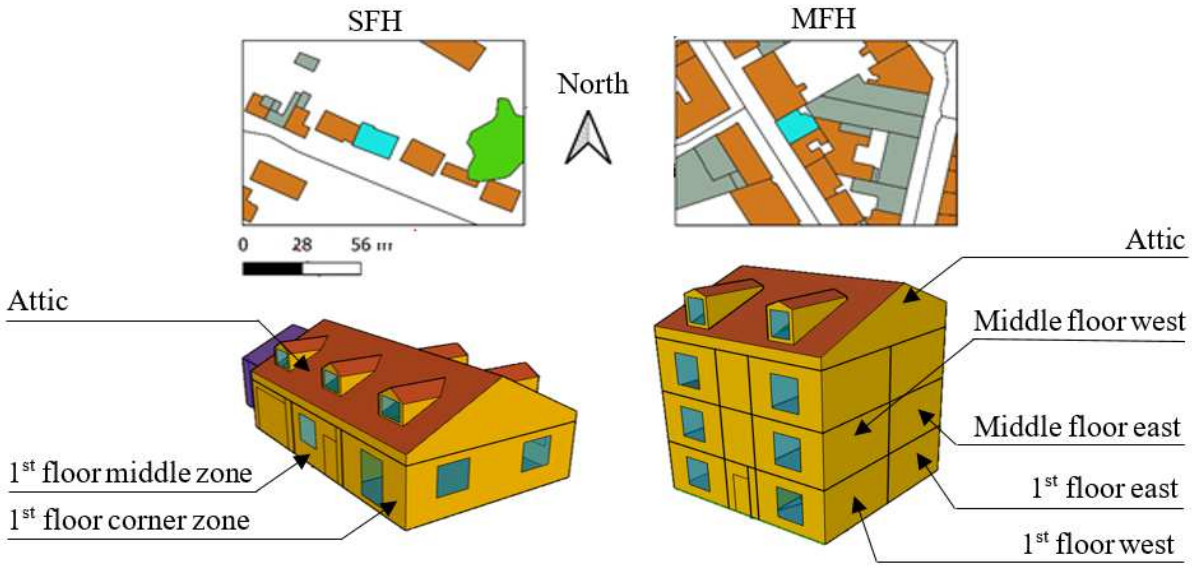

Figure 10: SFH and MFH buildings and their urban context

Figure 14, demonstrates the percentage of hours when indoor air temperature and humidity ratio were within each polygon of Givoni bioclimatic index for five summer months in MFH and SFH with two different weather files.

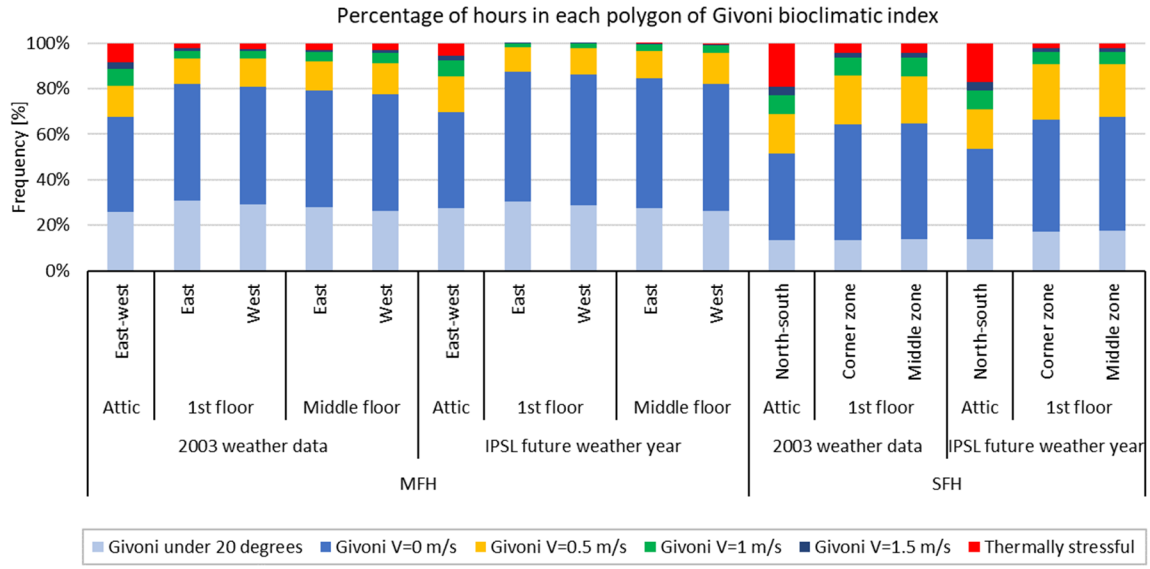

Figure 11: Percentage of hours indoor air temperature and relative humidity were within each polygon of Givoni bioclimatic index

Givoni diagram presented in Figure 10, assess summer thermal comfort of occupants subjected to various indoor air velocities. This index was selected primarily because installation of a ceiling or a portable fan is the first response of occupants to extreme temperature in naturally ventilated houses when passive strategies fail to provide expected comfort. Temperature, humidity ratio and indoor air velocity are the main parameters involved in comfort evaluation with this index. With weather data of 2003, approximately 20% and 10% of hourly data points in attics of SFH and MFH were outside polygon four (v=1.5 m/s), respectively. With IPSL-SMHI weather file, 17% of hourly data points in the attic of SFH and 4% in the attic of MFH were outside of polygon four (v=1.5 m/s).

Below, Figure 15 depicts degree-hours and percentage of hours indoor operative temperature in selected zones that exceeded maximum allowable operative temperatures in EN 16798-1.

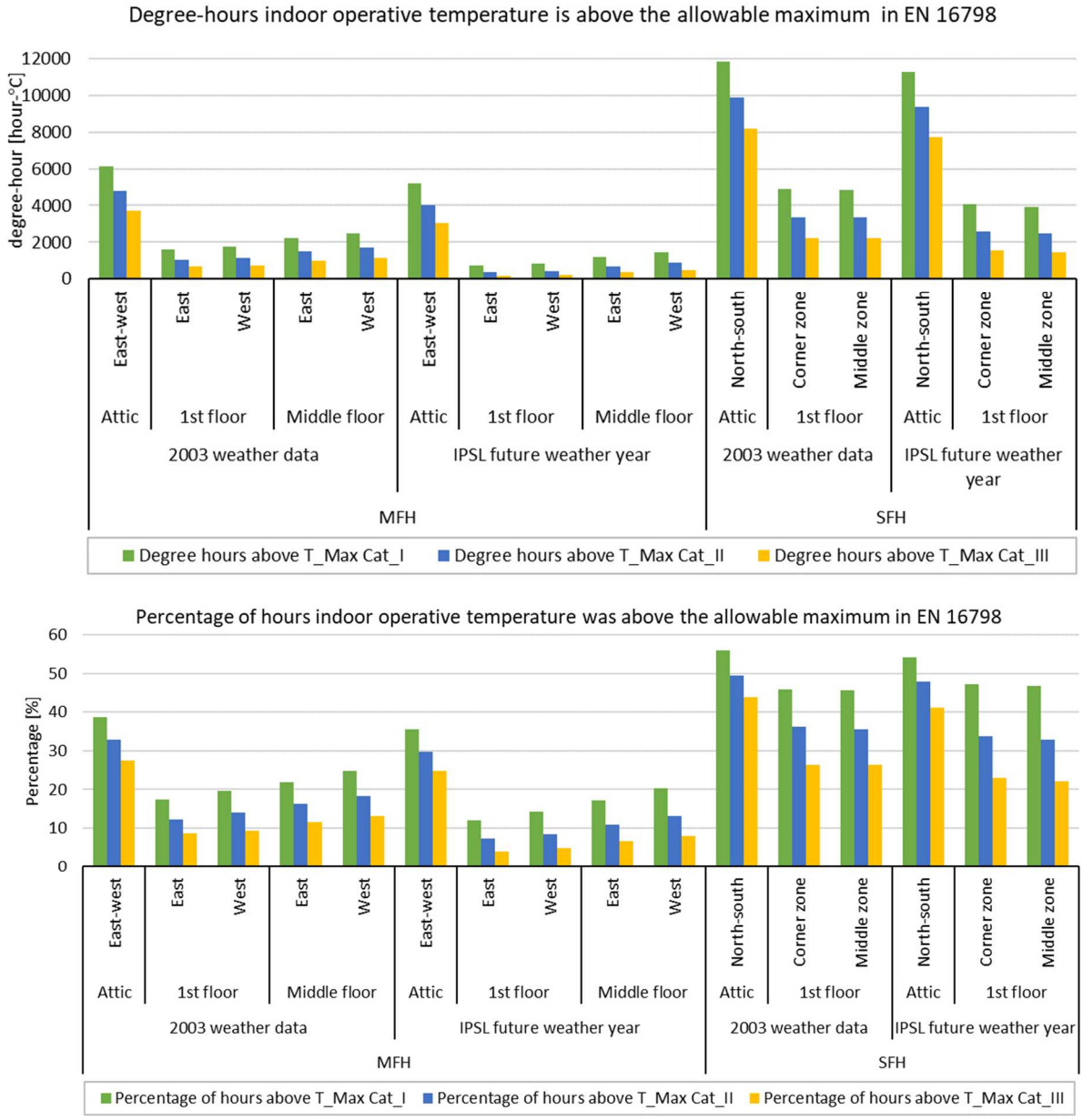

Figure 12: Degree hours and percentage of hours indoor operative temperature exceeded maximum adaptive thresholds of EN 16798-1

Degree-hours, although is an excellent unit of measurement that shows both the frequency and intensity of exceeding operative temperature, but it fails to create a picture on the scale of discomfort for practitioners due to the absence of a degree-hour threshold. Hence, percentage of exceeding hours is proposed. For instance, with 2003 weather file, indoor operative temperature in the attic of MFH exceeded maximum allowable threshold of EN 16798-1

category II by 4700 degree-hours during five summer months. This statement although accurate does not give a meaningful picture of discomfort level to practitioners or users. However, practitioners may find it easier to imagine the level of discomfort if they hear that indoor operative temperature in the attic of MFH exceeded maximum allowable threshold of EN 16798-1 category II, 31% of summertime. Presenting discomfort with percentage and degree-hours for five summer months are good indicators to represent the overall comfort performance of a thermal zone or building to overheating but they also fail to depict the intensity and severity of heatwave or its consequences on indoor thermal conditions.

Therefore, we decided to illustrate indoor thermal conditions with the constant temperature of 27 °C degrees as well. In this index, peak indoor air temperature and maximum number of consecutive hours when indoor air temperature exceeds 27 °C are calculated. Figure 16, presented below, shows peak indoor air temperature and maximum consecutive hours when temperature is above 27°C with both weather files and in both buildings.

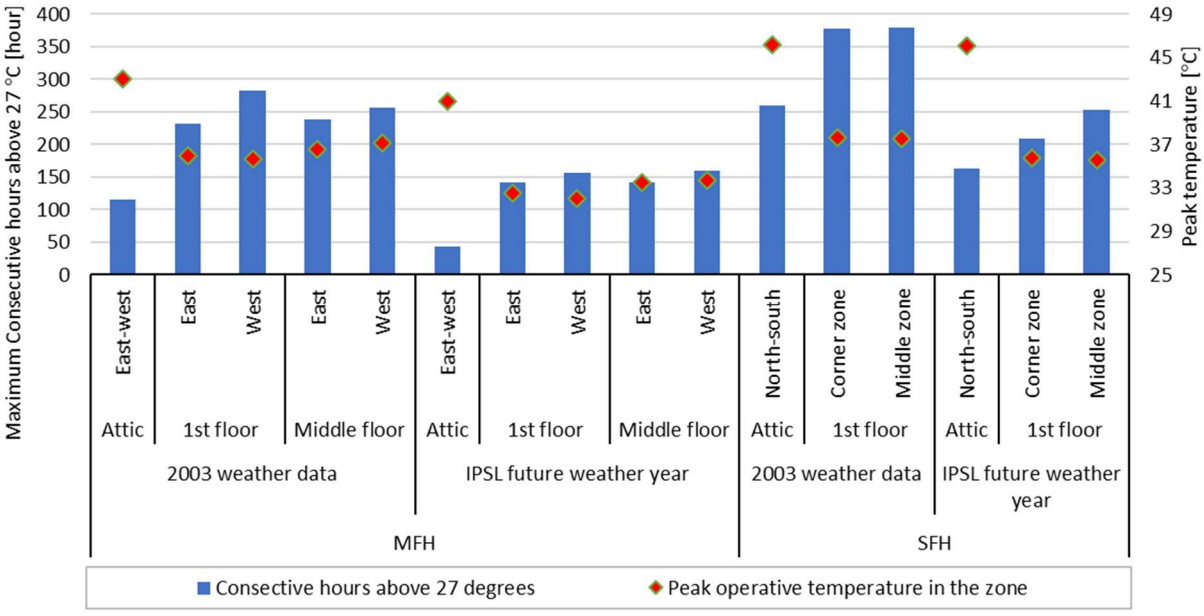

Figure 13: Peak indoor temperature and maximum consecutive hours above 27°C.

Similar to indices presented earlier, peak indoor temperatures are higher in the attics compared to other zones. Inversely, number of maximum consecutive hours above the selected threshold is considerably lower in the attics compared to other zones.

As can be seen in Figure 14 to Figure 16, attic of SFH oriented north-south experiences the worst indoor temperature conditions compared to other zones in the first floor of SFH. Indoor peak temperature in the attic of SFH reaches up to 46 °C during the heatwave with 2003 weather file. However, the duration of consecutive hours that temperature is above 27 °C is significantly lower in the attic of SFH in comparison to thermal zones in the first floor of SFH. This could be due to large direct exposure surface of attic to external environments. Large contact surface allows attic of SFH to experience rapid rise and drop in indoor temperature. Some may argue that it is because of smaller thermal capacity, but in simulation tool, thermal capacity of attic in SFH is twice as much as the thermal capacity of corner zone in the first floor of SFH. Attic of MFH, which is oriented east-west, also showed similar behaviour but the intensity of over-temperature is comparatively less than attic of SFH.

In contrast to SFH, roof and exterior walls of MFH have considerably larger U-values. MFH is also located in a more densely built urban area, which means it is more likely to be influenced by the UHI effect. MFH has two joint neighbours in the south and north orientations. West and east orientations are open and exposed to external environment. SFH, on the other hand, is almost entirely in contact with the external environment and main orientations are toward south and north. SFH also has a larger window to wall ratio than MFH, 13% versus 10%. Overall, MFH performs comparatively better than SFH in all zones under future climate scenario (IPSL-SMHI weather file) and during the heatwave (2003 weather file). This could mean that when it comes to summer overheating risks in naturally ventilated houses, solar heat gains through the window; contact surface of a thermal zone to

the external environment; and orientation play a more significant role than thermo-physical properties such as U-value or location of building within the city. This is in coherence with the findings of (Baba and Ge 2020; Fosas et al. 2018). In both buildings, air inflow rate, shading rate and percentage, occupancy and plug load were assumed the same.

Comparing thermal comfort indices shows that Givoni bioclimatic index, due to initial assumptions on indoor air velocity may underestimate indoor overheating intensity compared to EN16798-1 and 27 °C degrees fixed temperature. For instance, in the attic of SFH, with weather data of 2003, using Givoni bioclimatic index, the frequency of times that indoor air temperature and relative humidity are outside polygon two (v=0.5 m/s) is about 31 % of summertime. Whereas, EN 16798-1 for the same thermal zone shows that indoor operative temperature exceeding category-II is nearly 10000-degree-hours or 49% of the summer period. This reaches 56% in category-I and 43% in category-III. Under both climate conditions, this percentage considerably exceeds the 3% threshold recommended by CIBSE for free-running buildings (Chartered Institution of Building Services Engineers 2013). Considering uncertainties in the input data for different indices, it can be concluded that adaptive thermal comfort index better represents general thermal comfort performance in free-running buildings during summer months. However, when it comes to intensity assessment of indoor over-temperature conditions, maximum consecutive hours above a specific threshold and peak indoor temperature create a better picture.

High intensity of heatwave in the summer period and higher number of HDD in 2003 weather data indicate that observed weather data of 2003 contains a higher discrepancy compared to IPSL-SMHI and therefore is more suitable for the evaluation of buildings to heatwaves but it might be overestimating energy demand for heating under future climate scenario.

4 Limitations and prospects

In this study, the raw data of all necessary climate variables used to construct typical weather data for the future are not bias-adjusted, therefore only a comparative assessment can be done with them. In addition, the thresholds used in heatwave detection, are fixed absolute thresholds for maximum and minimum daily temperatures and are based on the worst historical heatwave event. In future studies, for France or any other locations around the world, other methods of heatwaves measurement could also be used.

Furthermore, comparative analysis of weather files in this study was focused on medium future and on typical weather files. Further study is suitable to perform a comparative analysis of observed heatwave weather data of 2003 with near, and far future weather files, and with artificially generated extreme hot years. It is also worthwhile to note that the 2003 heatwave data may be suitable for overheating assessment in France but the application of historical heatwave data in other locations deserves further research.

Further research is suggested in the creation of Extreme Hot Year weather files from EURO-CORDEX to be compared with historical extreme weather years, and performing sensitivity analysis to determine if passive strategies help to reduce overheating risk in free-floating buildings that are located in temperate climate regions, such as our case study city.

5 Conclusions

In the first part of this paper, a methodology/workflow was described to generate yearly and typical ready-to-use weather files for BPS using EURO-CORDEX database of dynamically downscaled climate data of the past, present, and future.

We generated three FTWYs using this methodology, then compared them with future weather file of Meteonorm 2050, and measured weather data of 2003. Comparative analysis of future weather files showed a difference not only between the weather files that were generated by

DDS or ESD approaches but also between different DDS files themselves. This difference was demonstrated by statistical distribution plots of monthly air temperature, relative humidity and global horizontal irradiance in each weather file.

This comparative analysis also showed that the intensity of heatwave observed in 2003 is higher than typical hot days in the medium future for our case study city. However, the application of this conclusion in other regions requires further study.

The second part of the study investigated indoor overheating in two buildings that have distinct morphological and thermo-physical characteristics in Nantes, France, with 2003 heatwave weather data and with a typical medium future weather data, measuring indoor overheating in five summer months. Buildings were modelled in Trnsys v.17 and the two weather files used in simulations were modified for each building individually by UWG to take into account the effect of UHI.

Results revealed that solar heat gains through the window, contact surface of a thermal zone to the external environment, and orientation play a significant role in summer over-temperature vulnerability compared to U-value. It was also noted that buildings located in sparsely built areas could be even more vulnerable to extreme summer temperatures in comparison to those located in densely built urban areas, which receive less direct solar irradiance.

Three indicators (Givoni bioclimatic index, EN 16798-1, and constant temperature of 27 °C) were used to measure indoor overheating rate. Results of comparison between comfort indices showed that adaptive index better represents general thermal comfort performance in free-running buildings during summer months. However, when it comes to intensity assessment of indoor over-temperature conditions, maximum consecutive hours above a specific threshold and peak indoor temperature should also be included.

Overall, this study provided a deeper understanding into the analysis of climate change effect and heatwaves on indoor overheating in naturally ventilated residential buildings considering urban heat island effect, different weather data, different climate models and, different measurement indices.

Python Script Availability: Following Python scripts are available from the corresponding author, for academic purposes, upon request: Python script to plot psychometric chart and calculate points inside each polygon of Givoni bioclimatic index; Python script to download historical weather data of French weather stations and write them on an epw. file; Python script to extract yearly weather data from EURO-CORDEX NetCDF files; Python script to assemble typical weather file from yearly weather data.

References

Baba, Fuad Mutasim, and Hua Ge. 2020. 'Overheating Risk of a Single-Family Detached House Built at Different Ages under Current and Future Climate in Canada' eds. J. Kurnitski and T. Kalamees. *E3S Web of Conferences* 172: 02004.

Bande, Lindita et al. 2019. 'Validation of UWG and ENVI-Met Models in an Abu Dhabi District, Based on Site Measurements'. *Sustainability* 11(16): 4378.

Battersby, Stephen. 2016. *Clay's Handbook of Environmental Health.* New York: Taylor and Francis. http://public.ebookcentral.proquest.com/choice/publicfullrecord.aspx?p=4578981 (November 3, 2021).

Bhatnagar, Mayank, Jyotirmay Mathur, and Vishal Garg. 2018. 'Determining Base Temperature for Heating and Cooling Degree-Days for India'. *Journal of Building Engineering* 18: 270–80.

Borgeson, Sam, and Gail Brager. 2011. 'Comfort Standards and Variations in Exceedance for Mixed-Mode Buildings'. *Building Research & Information* 39(2): 118–33.

Brasche, Sabine, and Wolfgang Bischof. 2005. 'Daily Time Spent Indoors in German Homes – Baseline Data for the Assessment of Indoor Exposure of German Occupants'. *International Journal of Hygiene and Environmental Health* 208(4): 247–53.

Bueno, Bruno, Aiko Nakano, and Leslie Norford. 2015. 'Urban Weather Generator: A Method to Predict Neighborhood-Specific Urban Temperatures for Use in Building Energy Simulations'. In *12th Symposium on the Urban Environment*, , 6. http://www.meteo.fr/icuc9/LongAbstracts/udc5-4-6531531_a.pdf.

Bueno, Bruno, Leslie Norford, Julia Hidalgo, and Grégoire Pigeon. 2013. 'The Urban Weather Generator'. *Journal of Building Performance Simulation* 6(4): 269–81.

Carlucci, Salvatore, and Lorenzo Pagliano. 2012. 'A Review of Indices for the Long-Term Evaluation of the General Thermal Comfort Conditions in Buildings'. *Energy and Buildings* 53: 194–205.

Chartered Institution of Building Services Engineers. 2013. *The Limits of Thermal Comfort Avoiding Overheating in European Buildings ; CIBSE TM52: 2013*. London: CIBSE.

Civel, Edouard, and Jeremy Elbeze. 2016. 'Energy Efficiency in French Homes : How Much Does It Cost ?' *Climate Economics Chair of Paris-Dauphine University*: 30.

Daniela, Jacob et al. 2020. 'Regional Climate Downscaling over Europe: Perspectives from the EURO-CORDEX Community'. *Regional Environmental Change* 20(2): 51–66.

Doherty, Sarah et al. 2018. *National Climate Assessment Report. Chapter 2: Our Changing Climate*. https://nca2018.globalchange.gov/chapter/2/ (August 4, 2021).

EN 16798-1. 2019. 'Energy Performance of Buildings - Ventilation for Buildings - Part 1: Indoor Environmental Input Parameters for Design and Assessment of Energy Performance of Buildings Addressing Indoor Air Quality, Thermal Environment, Lighting and Acoustics'.

Epstein, Yoram, and Daniel S. Moran. 2006. 'Thermal Comfort and the Heat Stress Indices'. *Industrial Health* 44(3): 388–98.

Erlandsen, Helene Birkelund et al. 2020. 'A Hybrid Downscaling Approach for Future Temperature and Precipitation Change'. *Journal of Applied Meteorology and Climatology* 59(11): 1793–1807.

Fosas, Daniel et al. 2018. 'Mitigation versus Adaptation: Does Insulating Dwellings Increase Overheating Risk?' *Building and Environment* 143: 740–59.

Green, Helen K. et al. 2016. 'Mortality during the 2013 Heatwave in England – How Did It Compare to Previous Heatwaves? A Retrospective Observational Study'. *Environmental Research* 147: 343–49.

Hamdy, Mohamed, Salvatore Carlucci, Pieter-Jan Hoes, and Jan L.M. Hensen. 2017. 'The Impact of Climate Change on the Overheating Risk in Dwellings—A Dutch Case Study'. *Building and Environment* 122: 307–23.

Hosseini, Mirata, Anahita Bigtashi, and Bruno Lee. 2021. 'Generating Future Weather Files under Climate Change Scenarios to Support Building Energy Simulation – A Machine Learning Approach'. *Energy and Buildings* 230: 110543.

IPCC. 2021. *Climate Change 2021: The Physical Science Basis. Contribution of Working Group I to the Sixth Assessment Report of the Intergovernmental Panel on Climate Change*. [Masson-Delmotte, V., P. Zhai, A. Pirani, S.L. Connors, C. Péan, S. Berger, N. Caud, Y. Chen, L. Goldfarb, M.I. Gomis, M. Huang, K. Leitzell, E. Lonnoy, J.B.R. Matthews, T.K. Maycock, T. Waterfield, O. Yelekçi, R. Yu,and B. Zhou (eds.)]. Cambridge University Press. https://www.ipcc.ch/report/ar6/wg1/#SPM.

ISO 15927-4. 2005. '[EN ISO 15927-4_2005] -- Hygrothermal Performance of Buildings. Calculation and Presentation of Climatic Data. Hourly Data for Assessing the Annual Energy Use for Heating and .Pdf'.

Jacob, Daniela et al. 2014. 'EURO-CORDEX: New High-Resolution Climate Change Projections for European Impact Research'. *Regional Environmental Change* 14(2): 563–78.

Kamal, Athar et al. 2021. 'Impact of Urban Morphology on Urban Microclimate and Building Energy Loads'. *Energy and Buildings*: 111499.

Kumar, Sanjay et al. 2019. 'Comparative Study of Thermal Comfort and Adaptive Actions for Modern and Traditional Multi-Storey Naturally Ventilated Hostel Buildings during Monsoon Season in India'. *Journal of Building Engineering* 23: 90–106.

Lauzet, Nicolas, Dasaraden Mauree, Thibaut Colinart, and Marjorie Musy. 2018. 'Construction of reusable urban microclimate weather files for BPS/Construction d'un fichier microclimatique urbain utilisable en STD. (in French)'. : 8.

Lomas, Kevin J., and Stephen M. Porritt. 2017. 'Overheating in Buildings: Lessons from Research'. *Building Research & Information* 45(1–2): 1–18.

Machard, Anaïs et al. 2020. 'A Methodology for Assembling Future Weather Files Including Heatwaves for Building Thermal Simulations from the European Coordinated Regional Downscaling Experiment (EURO-CORDEX) Climate Data'. *Energies* 13(13): 3424.

Malet-Damour, Bruno. 2012. 'Impact of the Climate on the Design of Low-Energy Buildings for Australia and Reunion Island'. In *12th Conference of International Building Performance Simulation Association*, Sydney, 2867–73. hal-00768497.

Manoli, Gabriele et al. 2019. 'Magnitude of Urban Heat Islands Largely Explained by Climate and Population'. *Nature* 573(7772): 55–60.

Maraun, Douglas. 2016. 'Bias Correcting Climate Change Simulations - a Critical Review'. *Current Climate Change Reports* 2(4): 211–20.

McCartney, Kathryn J, and J Fergus Nicol. 2002. 'Developing an Adaptive Control Algorithm for Europe'. *Energy and Buildings* 34(6): 623–35.

Mitchell, Dann, Kai Kornhuber, Chris Huntingford, and Peter Uhe. 2019. 'The Day the 2003 European Heatwave Record Was Broken'. *The Lancet Planetary Health* 3(7): e290–92.

Mitchell, Rachel, and Sukumar Natarajan. 2019. 'Overheating Risk in Passivhaus Dwellings'. *Building Services Engineering Research and Technology* 40(4): 446–69.

Moazami, Amin, Vahid M. Nik, Salvatore Carlucci, and Stig Geving. 2019. 'Impacts of Future Weather Data Typology on Building Energy Performance – Investigating Long-Term Patterns of Climate Change and Extreme Weather Conditions'. *Applied Energy* 238: 696–720.

Nicol, J. Fergus, Jake Hacker, Brian Spires, and Hywel Davies. 2009. 'Suggestion for New Approach to Overheating Diagnostics'. *Building Research & Information* 37(4): 348–57.

Nicol, J.F. 1974. 'An Analysis of Some Observations of Thermal Comfort in Roorkee, India and Baghdad, Iraq'. *Annals of Human Biology* 1(4): 411–26.

Ouzeau, G. et al. 2016. 'Heat Waves Analysis over France in Present and Future Climate: Application of a New Method on the EURO-CORDEX Ensemble'. *Climate Services* 4: 1–12.

Petrou, Giorgos et al. 2019. 'The Summer Indoor Temperatures of the English Housing Stock: Exploring the Influence of Dwelling and Household Characteristics'. *Building Services Engineering Research and Technology* 40(4): 492–511.

P.Tootkaboni, Mamak, Ilaria Ballarini, Michele Zinzi, and Vincenzo Corrado. 2021. 'A Comparative Analysis of Different Future Weather Data for Building Energy Performance Simulation'. *Climate* 9(2): 37.

Pyrgou, Andri et al. 2017. 'On the Effect of Summer Heatwaves and Urban Overheating on Building Thermal-Energy Performance in Central Italy'. *Sustainable Cities and Society* 28: 187–200.

Raei, Ehsan et al. 2018. 'GHWR, a Multi-Method Global Heatwave and Warm-Spell Record and Toolbox'. *Scientific Data* 5(1): 180206.

Rahif, R., D. Amaripadath, and S. Attia. 2021. 'Review on Time-Integrated Overheating Evaluation Methods for Residential Buildings in Temperate Climates of Europe'. *Energy and Buildings* 252: 111463.

Ramon, Delphine et al. 2019. 'Future Weather Data for Dynamic Building Energy Simulations: Overview of Available Data and Presentation of Newly Derived Data for Belgium'. In *Energy Sustainability in Built and Urban Environments*, Energy, Environment, and Sustainability, eds. Emilia Motoasca, Avinash Kumar Agarwal, and Hilde Breesch. Singapore: Springer Singapore, 111–38. http://link.springer.com/10.1007/978-981-13-3284-5_6 (May 20, 2021).

Robinson, Darren, and Frédéric Haldi. 2008. 'Model to Predict Overheating Risk Based on an Electrical Capacitor Analogy'. *Energy and Buildings* 40(7): 1240–45.

Salvati, Agnese, Massimo Palme, and Luis Inostroza. 2017. 'Key Parameters for Urban Heat Island Assessment in A Mediterranean Context: A Sensitivity Analysis Using the Urban Weather Generator Model'. *IOP Conference Series: Materials Science and Engineering* 245: 082055.

Thiis, Thomas K. et al. 2017. 'Monitoring and Simulation of Diurnal Surface Conditions of a Wooden Façade'. *Procedia Environmental Sciences* 38: 331–39.

Wagner, Vérène. 2018. 'Evolution of heatwaves and associated mortality in France, 2004-2014/Évolution des vagues de chaleur et de la mortalité associée en France, 2004-2014 (in French)'. : 6.

WMO. 2020. *State of the Global Climate 2020*. World Meteorological Organization, 2021. https://library.wmo.int/doc_num.php?explnum_id=10618.

Yang, Jun et al. 2019. 'Heatwave and Mortality in 31 Major Chinese Cities: Definition, Vulnerability and Implications'. *Science of The Total Environment* 649: 695–702.

Future climate & heatwave weather data

- 3 dynamically downscaled future typical weather files of median future (2040-2070) from RCP 8.5 emission scenario.
- Measured weather data of 2003 exceptional heatwave.
- Future weather file from meteonorm for 2050, RCP 8.5 emission scenario.

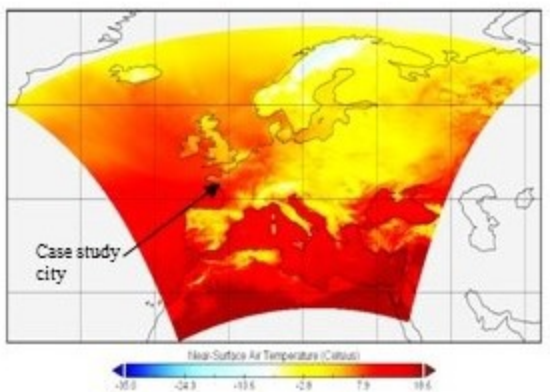

Urban heat island effect on two types of buildings

Urban morphology parameters in 200 meter radius for UWG:

- Average building height.
- Build density.
- Tree Cover ratio.
- Grass cover ratio.
- Vertical to horizontal area ratio.
- Year of construction.
- Climate zone: zone 4A for both buildings

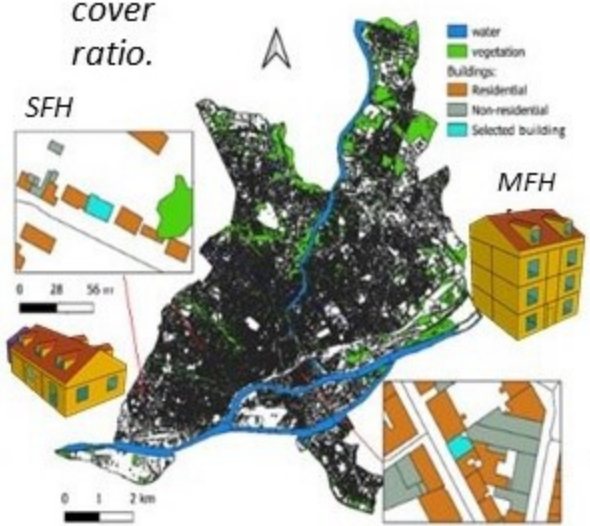

Building performance evaluation indices

- Givoni bioclimatic index.

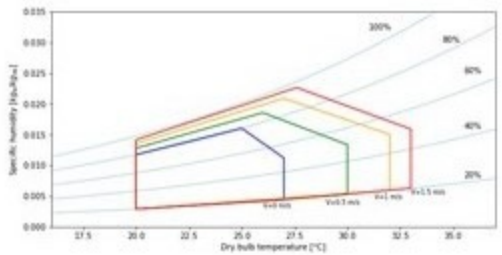

- EN 16798-1 adaptive index.

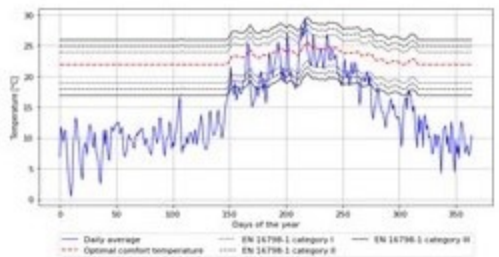

- Maximum consecutive hours above 27 °C & Peak indoor temperature.

Key findings

- Temperature in a typical summer in medium future (2040 -2070) is likely not as intense as the heatwave of 2003 for Nantes, France.
- Buildings located in sparsely built locations that are less affected by UHI are also at risk of overheating
- Results confirm it is better to use two weather files and at least two indoor overheating indices to evaluate a building's summer performance.